~~USS-10~~

dyf-69325 NI

TECHNICAL REPORT

STUDIES OF HYPERSONIC VISCOUS FLOWS OVER A BLUNT BODY AT LOW REYNOLDS NUMBER

By: Sang-Wook Kang

CAL No. AI-2187-A-9

Prepared for:

National Aeronautics and Space Administration
Goddard Space Flight Center
Greenbelt, Maryland 20771

Contract No. NAS5-9978
September 1968

CORNELL AERONAUTICAL LABORATORY, INC.
OF CORNELL UNIVERSITY, BUFFALO, N. Y. 14221

CORNELL AERONAUTICAL LABORATORY, INC.
BUFFALO, NEW YORK 14221

STUDIES OF HYPERSONIC VISCOUS FLOWS OVER A BLUNT BODY AT LOW REYNOLDS NUMBER

CAL Report No. AI-2187-A-9

September 1968

Prepared For:
NATIONAL AERONAUTICS AND SPACE ADMINISTRATION
GODDARD SPACE FLIGHT CENTER
GREENBELT, MARYLAND 20771

PREPARED BY: Sang-Wook Kang
Sang-Wook Kang

APPROVED BY: J. Gordon Hall
J. Gordon Hall, Head
Aerodynamic Research Department

FOREWORD

The work described in this report was supported by the National Aeronautics and Space Administration, Goddard Space Flight Center, under Contract NAS 5-9978. The author wishes to acknowledge the useful discussions with Dr. M. G. Dunn, and the assistance of Mr. J. R. Moselle in obtaining the numerical solutions.

ABSTRACT

The effects of mass injection on the viscous hypersonic shock layer in the forebody region (downstream as well as the stagnation point) of a blunt body are theoretically analyzed for a non-reacting gas in the incipient-merged layer regime. Both the normal and the streamwise components of the Navier-Stokes equations, along with the energy equation, are considered under the thin shock-layer assumption. After a suitable coordinate transformation, nonsimilar solutions are obtained by application of an integral method for blowing rates ranging from zero to as large as the free-stream mass flux $(\rho_\infty U_\infty)$. Significant influences of blowing on the character of the viscous shock layer are observed.

TABLE OF CONTENTS

LIST OF SYMBOLS

a	Body nose radius
A	Skin-friction parameter, $(\partial U/\partial F)_b$
B	Heat-transfer parameter, $(\partial \Theta/\partial F)_b$
C_F	Skin-friction coefficient, Eq. (23)
C_H	Stanton number, Eq. (22)
F	Transformed normal coordinate, Eq. (6)
f	Dimensionless stream function
G	Parameter for shock standoff distance, Eq. (6)
H	Total enthalpy, $h + (u^2+v^2)/2$
h	Static enthalpy
j	Unity for axisymmetric flow and zero for planar flow
k	Thermal conductivity
K^2	Rarefaction parameter, $\varepsilon(\rho_\infty U_\infty a/\mu_*)(T_*/T_o)$
L	$\equiv \int_0^1 U\,dF$
M_i	Integrals involving U and Θ, Sec. 2
N	Blowing parameter, $(\rho_b v_b)/(\rho_\infty U_\infty)$
p	Pressure
$\bar{p}_1$	$\equiv p/p_e$
Pr	Prandtl number
Q	$\equiv Pr\, K^2 G$
Q_1	$\equiv Q \cdot \sqrt{1-z^2}$
r	Distance from the axis to the body surface
T	Temperature

LIST OF SYMBOLS (Cont.)

t_b	$\equiv H_b/H_\infty$
U	Dimensionless streamwise velocity, $u/(U_\infty \cos\beta)$
u, v	Velocities in physical coordinates (Fig. 1)
x, y	Physical coordinates (Fig. 1)
z	$\equiv r/a$
β	Shock angle
Δ	Shock standoff distance (Fig. 1)
ε	$\equiv (\gamma-1)/(2\gamma)$
Θ	Enthalpy ratio, $(H-H_b)/(H_\infty-H_b)$
μ	Viscosity
ξ	Dimensionless streamwise distance, x/a
ρ	Density
ψ	Stream function

Subscripts

b	Body surface
e	Outer edge of the viscous shock layer
$*$	Reference condition
∞	Free-stream condition
o	Stagnation condition

1. INTRODUCTION

The purpose of the present analysis is to investigate theoretically the effects of mass injection on the viscous hypersonic flow in the forebody region (downstream as well as the stagnation point) of a blunt body in the incipient-merged layer regime. The rates of mass injection ("blowing") considered in the present paper range from zero, i.e., solid wall, to in some cases as large as the free-stream mass flux $(\rho_\infty U_\infty)$.

A brief description of the physical characteristics of the hypersonic low-Reynolds number flow as well as a short review of previous analyses will be given in this section, while the method of solution adopted in the present analysis and the discussion of results will be included in Secs. 2 and 3, respectively.

The viscous hypersonic flow at low Reynolds numbers has been a subject of interest[1-18] in recent years because the thin boundary-layer approximation can no longer be used in analyzing the flow around a blunt body at high altitudes.[1-4] Many analyses[1-3, 7-18] of the low Reynolds number flow are available for restricted geometries. While most of them treat the stagnation region of a blunt body, others are concerned with the sharp leading edge of a flat plate. No analyses are currently available for describing this low-density flow about a practical entry body. The problem is, however, important in that for the case of an Apollo body under typical reentry conditions, the thin boundary-layer assumption breaks down at altitudes greater than about 250,000 feet. At higher altitudes the influence of the transport properties is spread across the shock layer and even the shock wave itself may not be thin compared to the shock standoff distance. Thus, a different type of flow will exist at these rarefied conditions. Delineation of the various flow regimes has been proposed[1, 5] in terms of the degree of the rarefaction of the flow. Cheng[2] introduces a "rarefaction parameter", K^2 , in describing these flow regimes. It has been found from the analysis of the stagnation region[12] that the parameter K^2 may be used as a meaningful parameter even for the case of mass injection.

As the degree of rarefaction increases, intermolecular collisions become less frequent and molecules arriving at the body surface are unable to come into equilibrium with the surface. As a result, velocity and temperature discontinuities ("slip") may develop at the body surface. The effects of these wall-slip phenomena have been analyzed by Liu[15] and have been found to cause only a small change in the heat-transfer rate to the body and the shock standoff distance.

One aspect of the rarefaction of the viscous flows, i.e., low values of K^2 , is that the shock wave is no longer thin or discontinuous. As a result, the usual Rankine-Hugoniot relationship should be modified in order to account for the transport effects immediately behind the now-thickened shock wave. This has been analyzed and the modified Rankine-Hugoniot relationships have been obtained by Cheng.[2]

The effects of mass injection in the stagnation region of a blunt body have been considered by Goldberg,[10, 11] by Chen, Aroesty and Mobley,[12] and by Kang and Dunn.[13] Their results demonstrate increasing shock standoff distance and decreasing heat transfer with increasing injection rates. However, these changes are not as great at higher altitudes. Thus, for the rarefied-flow case, larger mass-injection rates are necessary to reduce the heat transfer coefficient by the same percentage as that for the thin-boundary-layer case.

No previous analyses are known to exist which treat the cases of blowing at locations away from the stagnation region of a blunt body. In the present paper this problem is formulated and analyzed by application of an integral-method approach. In an earlier paper,[13] this method was applied to a specialized case of the mass injection in the stagnation region, and good agreement with previous analyses[2, 12] was noted. The present paper constitutes an extension of the integral-method approach to the cases of mass injection in the downstream region of a blunt body at low Reynolds number.

2. FORMULATION OF ANALYSIS

2.1 General Discussion and Assumptions

An axisymmetric (or two-dimensional) flow over a blunt body with large blowing at the body surface is considered. The flow will be in the incipient merged-layer regime in which the Navier-Stokes equations may be used,[1,3,5] and the normal-momentum and the streamwise-momentum equations are simplified by assuming a very thin shock layer compared with the body radius. In addition, the body is taken to be spherical so that the radius of curvature a is a constant. The streamwise velocity component at the body surface u_b is assumed to be zero, implying no-slip condition which is reasonable for a cold-wall[3] case, i.e., $T_b \rightarrow 0$. However, it can be included as a nonzero quantity without difficulty.

The equations thus simplified are similar in form to the conventional boundary-layer equations with the important exceptions that the entire flow field is now viscous, instead of only a very thin layer near the wall, and that the normal pressure gradient may not be assumed negligible. The latter condition is associated with a non-negligible momentum change in the direction normal to the body surface.

In analyzing the present problem, the integral-method approach has been used in order to obtain approximate solutions because of the advantages of the method over the more complex exact method (which requires in most cases solution of the "two-point" boundary-value problem, or the use of an expansion scheme). These advantages are the ease of application and relatively small computation time. In addition, application of the integral method to the stagnation region with and without blowing[13] and to the flow past a sharp flat plate with zero mass injection[18] yielded reasonable results, further establishing the usefulness of the method. In the present analysis, results are obtained in the downstream as well as in the stagnation region of a blunt body for various values of the blowing rate $N(\xi)$, and of the "rarefaction parameter" K^2. Significant effects of mass injection on the viscous flow field are observed.

In order to simplify the analysis while retaining the essential features of the physical flow, the following specific assumptions are introduced: 1) a thin shock layer, 2) hypersonic flow, 3) non-reacting gas, 4) constant Prandtl number, 5) linear viscosity-temperature law, and 6) axisymmetric or two-dimensional flow.

2.2 Differential Equations

With the above assumptions, the Navier-Stokes equations for the viscous shock layer in the incipient-merged layer regime become[3] (see Fig. 1 for a description of the flow field):

Continuity:

$$\frac{\partial}{\partial x}(\rho u r^j) + \frac{\partial}{\partial y}(\rho v r^j) = 0 \tag{1}$$

Streamwise Momentum:

$$\rho u \frac{\partial u}{\partial x} + \rho v \frac{\partial u}{\partial y} = \frac{\partial}{\partial y}\left(\mu \frac{\partial u}{\partial y}\right) \tag{2}$$

Normal Momentum:

$$\rho \frac{u^2}{a} = \frac{\partial p}{\partial y} \tag{3}$$

Energy:

$$\rho u \frac{\partial H}{\partial x} + \rho v \frac{\partial H}{\partial y} = \frac{\partial}{\partial y}\left\{ \frac{\mu}{Pr} \frac{\partial}{\partial y}\left[H - (Pr - 1)\frac{u^2}{2} \right] \right\} \tag{4}$$

where the symbols are defined in the Nomenclature. It is noted that Cheng[2, 3] retains in Eq. (2) the $\partial p/\partial x$ term, which is second order in the incipient-merged layer regime, in order to allow extension of his analysis to the higher Reynolds number flow regime (details of the derivation of the above equations may be found in Ref. 3). The boundary conditions obtained using the modified Rankine-Hugoniot conditions[2] across the shock wave and taking into account the blowing at the body surface, are

at $y = 0$; $\quad u = 0, \quad v = v_b(x), \quad H = H_b(x), \quad p = p_b(x)$

at $y = \Delta$;

$$u = U_\infty \cos\beta - \frac{\mu_e}{\rho_\infty U_\infty \sin\beta}\left(\frac{\partial u}{\partial y}\right)_e$$

$$p \cong \rho_\infty U_\infty^2 \sin^2\beta$$

$$H = H_\infty - \frac{\mu_e}{Pr\, \rho_\infty U_\infty^2 \sin\beta} \frac{\partial}{\partial y}\left(H + \frac{Pr - 1}{2} u^2\right)_e \tag{5}$$

In the above boundary conditions the streamwise velocity component at the body surface u_b is assumed to be zero. It is also to be noted that the pressure distribution immediately behind the shock is Newtonian, in keeping with the thin shock-layer assumption.

The above differential equations are now transformed from the physical coordinate system to the $\xi - F$ coordinate system by defining

$$\xi = \frac{x}{a}, \quad F = \frac{1}{G}\int_0^y \frac{\rho}{\rho_\infty}\frac{dy}{a}, \quad G = \int_0^{\Delta(x)} \frac{\rho}{\rho_\infty}\frac{dy}{a} \tag{6}$$

In addition, we introduce the stream function ψ such that $\partial\psi/\partial x = -(1+j)(\pi r)^j \rho v$ and $\partial\psi/\partial y = (1+j)(\pi r)^j \rho u$, which automatically satisfies the continuity Eq. (1). A dimensionless stream function $f(\xi, F)$ is now obtained by putting $\psi \equiv (1+j)\rho_\infty U_\infty r(\pi r)^j f$, which yields the relationship $\partial f/\partial F = U G$, where $U \equiv u/(U_\infty z)$ and $z \equiv r/a \doteq \cos\beta$. Cheng[3] noted that z can be taken as either the shock surface or the body surface under the present thin shock-layer approximation. Therefore, so long as this assumption is valid, the error introduced is small, especially for flows around a blunt body.[3] It should be noted that the validity of this approximation should be verified for analyses treating mass injection, since blowing tends to thicken the shock layer and change the shock shape around a body.

Introduction of the new variables yields

$$-\frac{\rho v}{\rho_\infty U_\infty} = (1+j)\frac{dz}{d\xi} f + z\frac{\partial f}{\partial \xi} + r\left(\frac{\partial f}{\partial F}\right)\left(\frac{\partial F}{\partial x}\right)_y \tag{7}$$

and, from $\partial f/\partial F = U G$, we have

$$f(\xi, F) = f_b(\xi) + G(\xi)\int_0^F U\, dF \tag{8}$$

Transformation of Eqs (2), (3), (4) yields, assuming[2, 3]

$\mu = \mu_* (T/T_*)$:

Streamwise Momentum:

$$K^2 G \left[\frac{dz}{d\xi} \left(\frac{\partial f}{\partial F} \right)^2 + zG \left(\frac{\partial f}{\partial F} \right) \frac{\partial}{\partial \xi} \left(\frac{1}{G} \frac{\partial f}{\partial F} \right) - (1+j) \frac{dz}{d\xi} f \frac{\partial^2 f}{\partial F^2} - z \frac{\partial f}{\partial \xi} \frac{\partial^2 f}{\partial F^2} \right] = \frac{\partial^3 f}{\partial F^3} \tag{9}$$

Normal Momentum:

$$\frac{\partial p}{\partial F} = \rho_\infty U_\infty^2 \frac{z^2}{G} \left(\frac{\partial f}{\partial F} \right)^2 \tag{10}$$

Energy:

$$z \frac{dt_b}{d\xi} \frac{\partial f}{\partial F} (1-\theta) + z(1-t_b) \left(\frac{\partial f}{\partial F} \frac{\partial \theta}{\partial \xi} - \frac{\partial f}{\partial \xi} \frac{\partial \theta}{\partial F} \right) - (1+j)(1-t_b) \frac{dz}{d\xi} f \frac{\partial \theta}{\partial F}$$

$$= \frac{1-t_b}{P_r K^2 G} \cdot \frac{\partial^2 \theta}{\partial F^2} + \frac{P_r - 1}{P_r} \cdot \frac{2 z^2}{K^2 G^3} \cdot \frac{\partial}{\partial F} \left(\frac{\partial f}{\partial F} \cdot \frac{\partial^2 f}{\partial F^2} \right) \tag{11}$$

2.3 Boundary Conditions and Other Pertinent Relationships

The boundary conditions in the physical coordinate system, i.e., x-y plane, can be expressed in the transformed $\xi - F$ coordinate system. From Eq. (7), specializing to the body surface, i.e., $y = 0$ $(F = 0)$, we obtain

$$-\frac{\rho_b v_b}{\rho_\infty U_\infty} = (1+j) \frac{dz}{d\xi} f_b + z \frac{df_b}{d\xi} \tag{12}$$

where $U = 0$ at $F = 0$ is applied. The differential Eq. (12) can be solved to yield

$$f_b(\xi) = -\frac{\int_0^{\xi} z^j N(\xi)\, d\xi}{z^{1+j}} \tag{13}$$

For the special case, $\xi \rightarrow 0$, i. e., the stagnation point, $z \rightarrow 0$, Eq. (13) gives :

$$f_b(0) = -\frac{N(0)}{1+j} \tag{14}$$

On the other hand, application of the definition of ψ at $F = 1$, i. e., outer edge of the shock layer, yields $f_e = 1/(1+j)$. Also, from Eq. (5), we obtain, at $F = 1$:

$$U_e = 1 - \frac{1}{K^2 G\sqrt{1-z^2}}\left(\frac{\partial U}{\partial F}\right)_e$$

and

$$\theta_e = 1 - \frac{1}{P_r K^2 G\sqrt{1-z^2}}\left(\frac{\partial \theta}{\partial F}\right)_e \tag{15}$$

From the relationship $GU = (\partial f/\partial F)$, we obtain, using Eqs. (8) and (13):

$$GL = f_e - f_b = \frac{1}{1+j} + \frac{\int_0^{\xi} z^j N\, d\xi}{z^{1+j}} \tag{16}$$

where $L \equiv \int_0^1 U\, dF$ is introduced.

The physical coordinate y normal to the body surface is expressible in terms of the transformation variables such that $y/a = G\int_0^F (\rho_\infty/\rho)\, dF$. Using the ideal-gas relationship and after some rearrangement we obtain

$$\frac{y}{a} = \frac{\varepsilon G}{1-z^2}\int_0^F \left[\frac{t_b + (1-t_b)\theta}{p}\right] dF \tag{17}$$

where, from Eq. (10)

$$\bar{p}_1 \equiv \frac{p}{p_e} = 1 - \frac{z^2 G}{1-z^2} \int_F^1 U^2 dF \tag{18}$$

Thus the shock-layer thickness is

$$\frac{\Delta}{a} = \frac{\varepsilon G}{1-z^2} \int_0^1 \left[\frac{t_b + (1-t_b)\Theta}{\bar{p}} \right] dF \tag{19}$$

It is noted that a much simpler relationship exists at the stagnation point, since z is zero at $\xi = 0$. Then we have, at the stagnation point,

$$\frac{\Delta}{a} = \varepsilon G \int_0^1 [t_b + (1-t_b)\Theta] dF \tag{20}$$

which is equivalent to the results obtained in Refs. 2 and 12.

The streamline patterns as a function of ξ and F may be conveniently expressed as

$$\frac{\psi}{(1+j)\pi \rho_\infty U_\infty a^{1+j}} = z^{1+j}(\xi) \left[f_b(\xi) + G(\xi) \int_0^F U dF \right] \tag{21}$$

The heat transfer to the body is given in terms of the Stanton number C_H by:

$$C_H \equiv \frac{(k \partial T/\partial y)_b}{\rho_\infty U_\infty (H_\infty - H_b)} = \frac{B(\xi)}{P_r K^2 G(\xi)} \tag{22}$$

Finally, the skin friction is expressible in the present analysis to be

$$C_F' \equiv \frac{C_F}{\cos\beta} = \frac{(\mu \partial u/\partial y)_b}{\cos\beta \cdot (\rho_\infty U_\infty^2/2)} = \frac{2A(\xi)}{K^2 G(\xi)} \tag{23}$$

2.4 Application of Integral Method

The streamwise-momentum Eq. (9), the normal-momentum Eq. (10), and the energy Eq. (11) are now integrated from $F = 0$ to $F = 1$. By use of Eqs. (12), (15), (16), and after a series of rearrangements, the integration yields, in addition to Eq. (18) for the pressure distribution,

$$\frac{d}{d\xi}\left(z^{2+j} G M_1\right) = z^{1+j}\left(\frac{A}{K^2 G} + N + \frac{dz}{d\xi} G L\right) \tag{24}$$

and

$$\frac{d}{d\xi}\left[(1-t_b) z^{1+j} G M_2\right] = (1-t_b) z^{j}\left(\frac{B}{P_r K^2 G} + N\right) \tag{25}$$

where

$$M_1 \equiv \int_0^1 U(1-U)\,dF \quad , \quad M_2 \equiv \int_0^1 U(1-\Theta)\,dF$$

$$N(\xi) \equiv \frac{\rho_b \mu_b}{\rho_\infty \mu_\infty} \quad , \quad A \equiv \left(\frac{\partial U}{\partial F}\right)_b \quad , \quad B \equiv \left(\frac{\partial \Theta}{\partial F}\right)_b .$$

By substitution of the profiles of the streamwise velocity U and the total-enthalpy Θ (see Appendix for details of derivation) in the definitions of M_1 and M_2, we obtain expressions for these quantities in terms of two unknown parameters G and B. Other terms such as N, K^2, t_b, etc., are specified as known quantities and are functions of the streamwise distance ξ. The quantity L is obtained from Eq. (16) as a function of N, z and G. Thus, the problem is to determine from Eqs. (24) and (25) the two unknown parameters G and B which characterize the flow. The term G describes a measure of the shock-layer thickness in the transformed plane and the term B denotes the local heat-transfer parameter. Details of the determination of these quantities for various values of the mass-injection $N(\xi)$ and the rarefaction parameter K^2 and the discussion of the results obtained will be presented in the following section.

3. SOLUTIONS AND DISCUSSION OF RESULTS

3.1 Integration Procedure

For given values of the rarefaction parameter, the mass-injection rate distribution, and the surface-enthalpy ratio, the Eqs. (24) and (25) were numerically integrated along the streamwise distance to yield solutions in terms of the unknown parameters G and B. These parameters are used to describe other characteristic quantities of interest in the viscous hypersonic flow, such as the skin-friction coefficient, the heat-transfer coefficient, the pressure distribution, the velocity and the total-enthalpy profiles, and the streamline patterns in the viscous shock layer.

The numerical-integration scheme adopted was the Adams-Molton predictor-corrector method and the computation time for integration along ξ up to $\xi \cong 0.9$ for a single typical case, i.e., given values of K^2, t_b and N was about 0.7 minutes on the IBM 360 computer. Solutions were obtained for $t_b = 0.05$ (cold wall), K^2 between 0.1 and 10.0, and N varying from zero to as high as 1.0. It is noted that the examples included in the present paper are for uniform mass-injection cases along the body surface in order to emphasize the applicability of the present approach to the nonsimilar flow cases. However, the present approach is also applicable to arbitrary mass-injection distributions along the streamwise distance. All of these results display similar behaviors in response to mass injection, and only the results of a typical case ($K^2 = 1.0$) are presented in detail. However, the discussion encompasses the entire range of results obtained in the present analysis in the incipient-merged layer regime.

3.2 Heat Transfer and Skin Friction

Figures 2 and 3 show, respectively, the distributions of heat-transfer and skin-friction coefficients for uniform mass injection along the body surface for $K^2 = 0.1$, $K^2 = 1.0$, and $K^2 = 10.0$. It is seen from the figures that mass injection reduces both the heat transfer and the skin friction, a physically reasonable result which holds true also for thin boundary-layer flows.[19-25] It is interesting to note that at a lower Reynolds number $(K^2 = 0.1)$, the effect of blowing on the heat transfer, expressed in terms of the Stanton number C_H, and on the skin friction C_F' is small compared with the effect of blowing at a higher Reynolds number $(K^2 = 10)$. Thus, larger blowing rates are required at $K^2 = 0.1$ to reduce the heat-transfer coefficient by the same percentage as that for $K^2 = 10$. This result may stem from the relative ineffectiveness of the low-density fluid existing at higher altitudes to respond to mass injection at the body surface. This is more clearly seen by taking the free-molecular limit, i.e., $K^2 \rightarrow 0$.

Since there are no intermolecular collisions in this regime, the effect of mass injection on heat transfer from a cold wall is zero for a unit thermal accommodation coefficient. This trend has been found to hold in the stagnation region from previous analyses,[12, 13] and the present analysis shows that it also holds true in the downstream region.

3.3 Surface Pressure Distributions

The surface pressure distributions along the body at various values of κ^2 are shown in Fig. 4 for uniform blowing rates. The Newtonian pressure distribution is also shown in the figure for comparison, since in the present analysis the pressure distribution at the outer edge of the shock layer is assumed to be Newtonian, in keeping with the thin shock-layer concept.[3] The surface pressure is less than the pressure behind the shock given by the Newtonian theory, because of centrifugal effects, even for zero mass injection. Another interesting result is the influence of mass injection on the pressure at the body surface. Physically, the mass is injected normal to the body surface, further enhancing the centrifugal effects of the flow. Thus, the surface pressure decreases with increasing mass injection, as shown in Fig. 4.

3.4 Streamline Patterns

The present analysis also yields the streamline patterns within the viscous shock layer for various mass-injection rates. Examples are shown in Figs. 5-7 for the $\kappa^2 = 1.0$ case. These results are both interesting and useful, since they afford a means of assessing the meaningfulness of the physical flow, and since the reasonableness of the streamline behavior should tend to confirm, at least qualitatively, the appropriateness of the present approach. Figure 5 gives the streamline distribution for the zero-blowing case, that is, solid wall. In this case, the mass flowing in the viscous shock layer consists entirely of the free-stream mass entering through the shock wave; thus the stagnation streamline becomes the dividing streamline along the body and coincides with the body surface. When mass is now injected uniformly along the body at the surface, the layer in the immediate vicinity of the body surface consists of the injected mass and the dividing streamline is now pushed outward from the body. The blowing case of 10 percent of the free-stream mass flux is shown in Fig. 6 and the case of 50 percent injection ($\mathcal{N} = 0.5$) is illustrated in Fig. 7. It is seen that the stagnation streamline is located on the axis of symmetry (stagnation line) and then follows the dividing streamline in the downstream direction, with the injected mass on one side and the freestream mass on the other. The thickening of the shock layer and the noticeably changed streamline patterns as a result of very large blowing are observed in Fig. 7. Since the present analysis is based on a thin shock-layer assumption, it should be kept in mind that the justification of this assumption comes into question when the viscous shock layer becomes very thick (due to blowing) compared with the characteristic length of the body, which in this case is the body nose radius. In the absence of a clear-cut criterion which validates or invalidates the thin shock-layer approximation, the typical result is included in Fig. 7 to illustrate qualitatively, if not quite quantitatively, the changes in the viscous flow field due to very large rates of mass injection along the body surface.

3.5 Velocity and Total-Enthalpy Profiles

Based on the values of the parameters G and B obtained from solution of the Eqs. (24) and (25), the profiles for the streamwise velocity and the total enthalpy have been constructed using the expressions given in the Appendix. These profiles are shown in Figs. 8 through 11 for $N = 0$ and $N = 0.1$ cases. Despite the polynomial approximation that has been used, it is seen that reasonable profile descriptions are obtained for both the streamwise velocity U and for the total enthalpy Θ. As the shock-layer thickness increases in the downstream direction, i.e., increasing ξ, the edge values of U and Θ show slight reduction, signifying the increased viscous and conduction effects in the shock-transition zone which modify the Rankine-Hugoniot conditions.[3]

3.6 Comparison with Other Results

In an earlier paper[13] treating the effects of blowing in the stagnation region by essentially the same integral approach, comparison was made with the more exact analyses (analytical or finite-difference method) for heat transfer and shock standoff distance in the stagnation region of a solid body surface[2] and also with mass injection.[12] These comparisons are included here (Figs. 12 and 13) for the sake of completeness. A further comparison of heat transfer is given in Fig. 14 which shows the effects of blowing for various values of K^2. It may be seen from these figures that the present results agree well with the more exact results[12] in the stagnation region.

Since no other downstream analyses (either exact numerical or experimental) have been found which treat the problem of viscous hypersonic flow over a blunt body with large and small blowing, it was not possible to make comparisons in the downstream region. However, Chow[18] has analyzed the rarefied flow past the sharp leading edge of a flat plate using the integral method. He compares his theoretical results with experimental data and finds good agreement. Although the validity of the integral-method rests on the soundness of the assumptions and the agreement with experiment or exact solutions, the lack of experimental data for rarefied, viscous flow downstream of the stagnation point makes extensive comparison with experiment impossible at this time. Nevertheless, the purpose of the present analysis has been insight rather than precise numerical calculations. Thus, based on the comparison mentioned previously and on the results obtained in the present analysis as shown in Figs. 2 through 14, it appears that the integral-method approach presented in this paper provides a simple and useful method in analyzing the rarefied, hypersonic, viscous flow over a blunt body with large and small rates of mass injection.

4. CONCLUSIONS

In summary, an analysis of the hypersonic, low Reynolds-number flow over a blunt body with blowing has been presented for a non-reacting gas in the incipient-merged layer regime by application of an integral method. Both the normal and the streamwise components of the Navier-Stokes equation and the energy equation have been considered under the thin shock-layer assumption. Solutions were obtained for various blowing rates and degrees of rarefaction in the downstream region as well as in the stagnation region. These results indicate significant effects of blowing and rarefaction on the heat-transfer rates, the skin friction, the streamline patterns, and the pressure distributions within the viscous shock layer in the forebody region of a blunt body. One major result is that, as the degree of rarefaction increases, larger blowing rates are required to produce significant effects on the flow.

REFERENCES

1. Probstein, R. F., and Kemp, N., "Viscous Aerodynamic Characteristics in Hypersonic Rarefied Gas Flow," Journal of the Aerospace Sciences, Vol. 29, No. 3, March 1960, pp. 174-192, 218.

2. Cheng, H. K., "Hypersonic Shock-Layer Theory of the Stagnation Region at Low Reynolds Number," Proceedings of the Heat Transfer and Fluid Mechanics Institute, 1961, pp. 161-175.

3. Cheng, H. K., "The Blunt-Body Problem in Hypersonic Flow at Low Reynolds Number," Rept. AF-1285-A-10, June 1963, Cornell Aeronautical Laboratory, Buffalo, New York.

4. Scala, S. M., "Hypersonic Viscous Shock Layer," ARS Journal, Vol. 29, No. 7, July 1959, pp. 520-522.

5. Hayes, W. D., and Probstein, R. F., Hypersonic Flow Theory, Academic Press, New York, 1959, pp. 375-395.

6. Cheng, H. K., "Viscous Hypersonic Blunt-Body Problems and the Newtonian Theory," Proceedings of the International Symposium on Fundamental Phenomena in Hypersonic Flow, edited by J. G. Hall, Cornell University Press, Ithaca, N. Y., 1966, pp. 90-131.

7. Ho, H. T., and Probstein, R. F., "The Compressible Viscous Layer in Rarefied Hypersonic Flow," Proceedings of the Second International Symposium on Rarefied Gas Dynamics, edited by L. Talbot, Academic Press, New York, 1961, pp. 525-552.

8. Oguchi, H., "Blunt Body Viscous Layer with and without Magnetic Field," The Physics of Fluids, Vol. 3, No. 4, April 1960, pp. 567-580.

9. Levinsky, E. S., and Yoshihara, H., "Rarefied Hypersonic Flow over a Sphere," ARS Progress in Astronautics and Rocketry: Hypersonic Flow Research, edited by F. D. Riddell, Vol. 7, Academic Press, New York, 1962, pp. 81-106.

10. Goldberg, L., and Scala, S. M., "Mass Transfer in the Hypersonic Low Reynolds Number Viscous Layer," Paper 62-80, Jan. 1962, Institute of Aerospace Sciences.

11. Goldberg, L., "The Structure of the Viscous Hypersonic Shock Layer," Rept. R65SD50, Dec. 1965, General Electric Co.

12. Chen, S. Y., Aroesty, J., and Mobley, R., "The Hypersonic Viscous Shock Layer with Mass Transfer," International Journal of Heat and Mass Transfer, Vol. 10, No. 9, Sept. 1967, pp. 1143-1158.

13. Kang, S. W., and Dunn, M. G., "Integral Method for the Stagnation Region of a Hypersonic Viscous Shock Layer with Blowing," AIAA Journal, to appear as a Technical Note, 1968.

14. Chung, P. M., "Hypersonic Viscous Shock Layer of Nonequilibrium Dissociating Gas," TR R-109, May 1961, NASA.

15. Liu, J. C. T., "The Effect of Wall Temperature on the Low Reynolds Number Hypersonic Stagnation Region Shock Layer," International Journal of Heat and Mass Transfer, Vol. 10, No. 1, Jan. 1967, pp. 83-95.

16. Tong, H., "Effects of Dissociation Energy and Vibrational Relaxation on Heat Transfer," AIAA Journal, Vol. 4, No. 1, Jan. 1966, pp. 14-18.

17. Bush, W. B., "On the Viscous Hypersonic Blunt-Body Problem," Journal of Fluid Mechanics, Vol. 20, Part 3, 1964, pp. 353-367.

18. Chow, W. L., "Hypersonic Rarefied Flow Past the Sharp Leading Edge of a Flat Plate," AIAA Journal, Vol. 5, No. 9, Sept. 1967, pp. 1549-1557.

19. Head, M. R., "An Approximate Method of Calculating the Laminar Boundary Layer in Two-Dimensional Flow," R & M 3123, March 1957, Aeronautical Research Council.

20. Kang, S. W., "An Integral Method for Three-Dimensional, Compressible, Laminar Boundary Layers with Mass Injection," Rept. AI-2187-A-5, May 1967, Cornell Aeronautical Laboratory, Buffalo, New York; also Kang, S. W., Rae, W. J., and Dunn, M. G., "Studies of Three-Dimensional, Compressible Boundary Layers on Blunt Lifting Entry Bodies," AGARD Specialists' Meeting on Hypersonic Boundary Layers and Flow Fields, May 1968, London, England.

21. Inger, G. R. and Gaitatzes, G. A., "Strong Blowing into Laminar Viscous Flows around Two-Dimensional and Axisymmetric Supersonic Bodies," Paper 68-719, June 1968, AIAA.

22. Morduchow, M., "On Heat Transfer over a Sweat-Cooled Surface in Laminar Compressible Flow with a Pressure Gradient," Journal of the Aeronautical Sciences, Vol. 19, No. 10, Oct. 1952, pp. 705-712.

23. Kang, S. W., Rae, W. J., and Dunn, M. G., "Effects of Mass Injection on Compressible, Three-Dimensional, Laminar Boundary Layers," AIAA Journal, Vol. 5, No. 10, Oct. 1967, pp. 1738-1745.

24. Libby, P. A., "The Homogeneous Boundary Layer at an Axisymmetric Stagnation Point with Large Rates of Injection," Journal of Aerospace Sciences, Vol. 29, No. 1, Jan. 1962, pp. 48-60.

25. Tien, C. L. and Gee, C., "Hypersonic Viscous Flow over a Sweat-Cooled Flat Plate," AIAA Journal, Vol. 1, No. 1, Jan. 1963, pp. 159-167.

APPENDIX

Streamwise Velocity Profile

For the transformed streamwise velocity profile U, assume a third-degree polynomial form:

$$U = a_1 F + a_2 F^2 + a_3 F^3 \tag{A1}$$

where the coefficients a_1, a_2, a_3 are to be determined from the boundary conditions. The boundary conditions used are the conservation of mass flux, Eq. (16), the streamwise-momentum equation, Eq. (9), specialized to the body surface ($F = 0$), and the modified Rankine-Hugoniot condition, Eq. (15). They are:

$$\begin{aligned} \int_0^1 U \, dF &= L , \\ \left(\frac{\partial^2 U}{\partial F^2}\right)_b &= K^2 G N \left(\frac{\partial U}{\partial F}\right)_b , \\ U_e &= 1 - \frac{1}{Q_2}\left(\frac{\partial U}{\partial F}\right)_e \end{aligned} \tag{A2}$$

where $Q_2 \equiv K^2 G \sqrt{1 - z^2}$. Substitution of Eq. (A1) with the first two conditions in Eq. (A2) yields, for the streamwise velocity profile:

$$U = 4 L F^3 + A (F + N_8 F^2 - N_9 F^3) \tag{A3}$$

where $N_8 \equiv K^2 G N / 2$, and $N_9 \equiv 2(1 + K^2 G N / 3)$. Combination of Eq. (A3) with the last condition in Eq. (A2) gives

$$A \equiv \left(\frac{\partial U}{\partial F}\right)_b = \frac{12 L + Q_2 (4L - 1)}{5 + 2N_8 + Q_2 (1 + N_8 / 3)} \tag{A4}$$

Total-Enthalpy Profile

For the profile of the total-enthalpy, we put

$$\Theta = b_1 F + b_2 F^2 + b_3 F^3 + b_4 F^4 \tag{A5}$$

where b_1, b_2, ..., are to be determined from the boundary conditions. These boundary conditions are obtained from matching Eq. (11) at the shock interface with the results obtained for the shock-transition zone,[3] from specializing Eq. (11) to the body surface, and from the modified Rankine-Hugoniot conditions. Thus we have

$$\left(\frac{\partial^2\Theta}{\partial F^2}\right)_e + Q_1\left(\frac{\partial\Theta}{\partial F}\right)_e = 0$$

$$\Theta_e = 1 - \frac{1}{Q_1}\left(\frac{\partial\Theta}{\partial F}\right)_e \tag{A6}$$

$$\left(\frac{\partial^2\Theta}{\partial F^2}\right)_b = QN\left(\frac{\partial\Theta}{\partial F}\right)_b$$

where

$$Q \equiv P_r K^2 G$$

$$Q_1 \equiv Q\sqrt{1-z^2}$$

Combination of Eqs. (A5) and (A6) yields, for the total-enthalpy profile

$$\Theta = \frac{F^3}{N_1}(N_2 - N_3 F) \tag{A7}$$

$$+ \frac{B}{N_1}\left[N_1 F + \frac{QNN_1}{2}F^2 - (N_4 + QNN_5)F^3 + (N_6 + QNN_7)F^4\right]$$

where

$$N_1 = 12 + 6Q_1 + Q_1^2 \quad , \qquad N_2 = 4Q_1(3+Q_1)$$

$$N_3 = 3Q_1(2+Q_1) \quad , \qquad N_4 = 3(2+Q_1)^2$$

$$N_5 = 8 + 5Q_1 + Q_1^2 \quad , \qquad N_6 = 2(3+3Q_1 + Q_1^2)$$

$$N_7 = \frac{1}{2}(6 + 4Q_1 + Q_1^2) .$$

The integral terms M_1 , M_2 are now obtained by using Eqs. (A3) for $\mho$ and Eq. (A7) for Θ to give:

$$M_1 \equiv \int_0^1 \mho(1-\mho)dF$$

$$= L\left(1-\frac{16}{7}L\right) + \frac{8}{7}AL\left(\frac{3}{5}+\frac{N_8}{6}\right) - \frac{A^2}{60}\left(22 + 13N_8 + 2N_8^2\right) \qquad \text{(A8)}$$

and

$$M_2 \equiv \int_0^1 \mho(1-\Theta)dF$$

$$= \frac{N_{10} + AN_{11}}{N_1} - \frac{B}{N_1}\left[N_{12} + A(N_{13} + QNN_{14})\right] \qquad \text{(A9)}$$

where

$$N_{10} = \frac{3L}{14}(56 + 10Q_1 + Q_1^2)$$

$$N_{11} = \frac{Q_1}{14}\left(\frac{37}{5} + 2N_8 + \frac{13}{10}Q_1 + \frac{Q_1N_8}{3}\right)$$

$$N_{12} = L\left[\frac{3}{35}(67+11Q_1+Q_1^2) + \frac{QN}{84}(78+12Q_1+Q_1^2)\right]$$

$$N_{13} = -\frac{N_1}{60}(4+N_8) + \frac{N_4}{7}\left(\frac{3}{5}+\frac{N_8}{6}\right) - \frac{N_6}{6}\left(\frac{1}{2}+\frac{N_8}{7}\right)$$

$$N_{14} = -\frac{N_1}{6}\left(\frac{1}{4}+\frac{N_8}{15}\right) + \frac{N_5}{7}\left(\frac{3}{5}+\frac{N_8}{6}\right) - \frac{N_7}{6}\left(\frac{1}{2}+\frac{N_8}{7}\right)$$

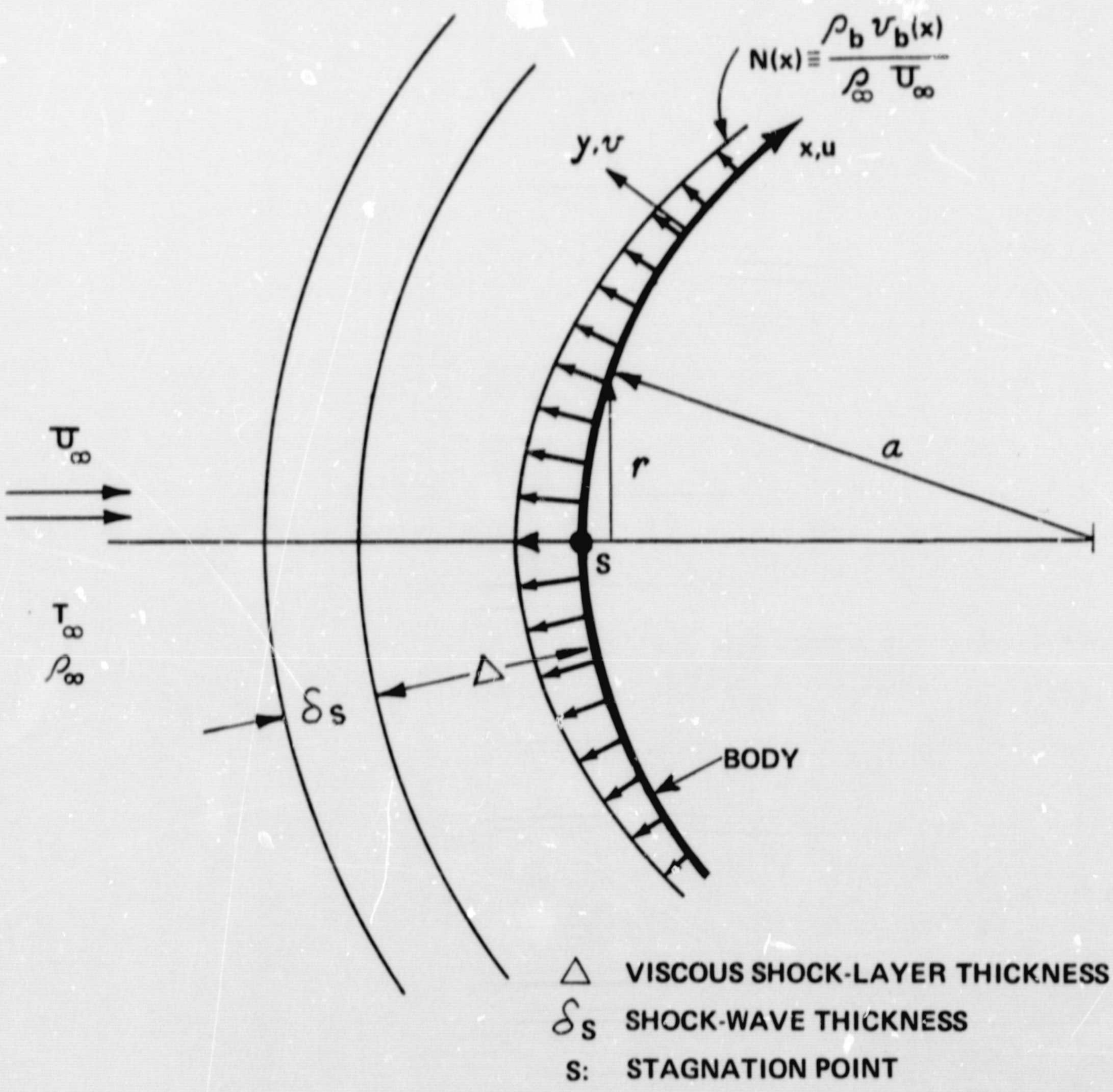

Figure 1 CO-ORDINATE SYSTEM

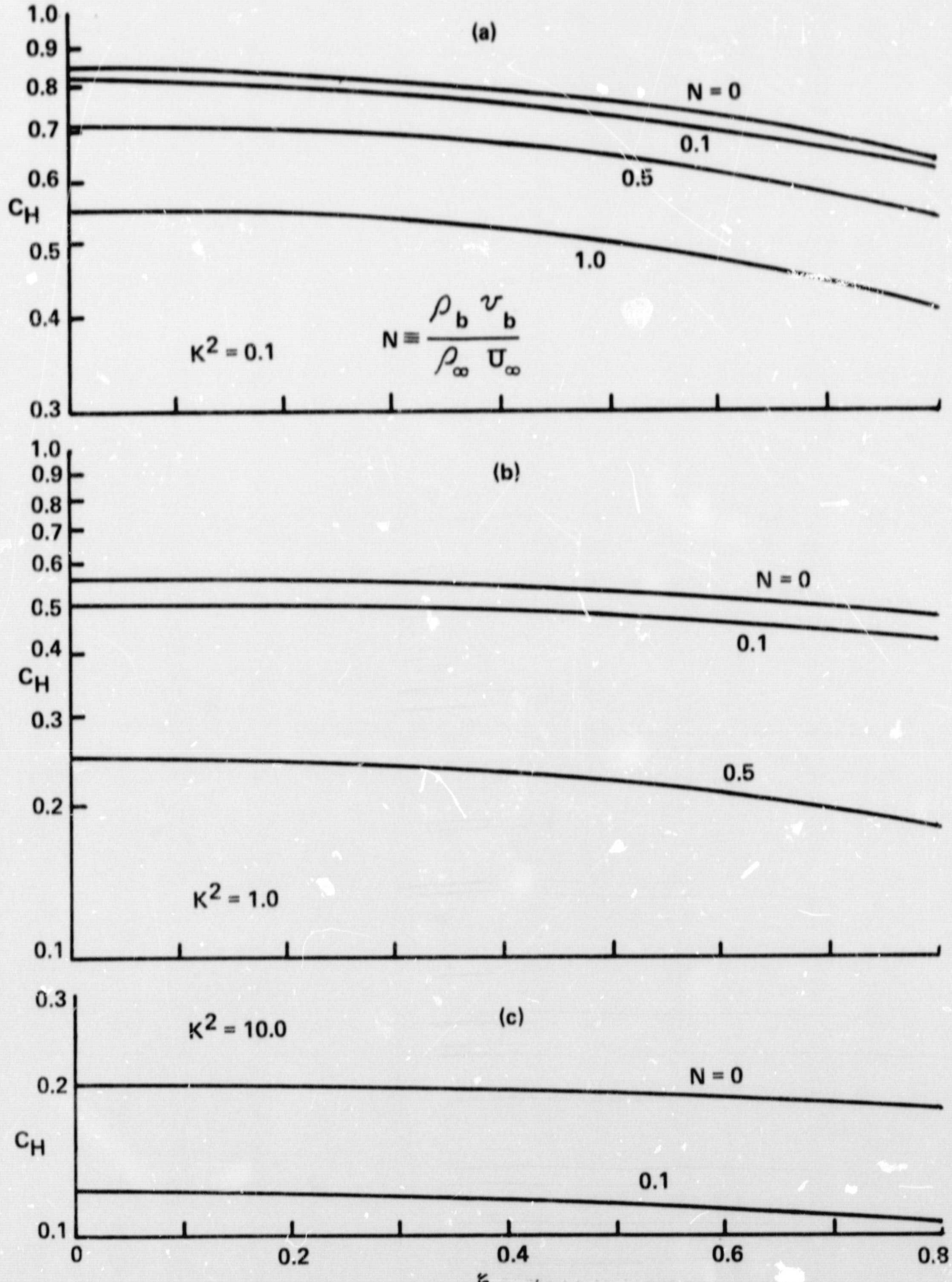

Figure 2 HEAT-TRANSFER DISTRIBUTIONS FOR VARIOUS MASS INJECTION RATES ALONG BODY SURFACE

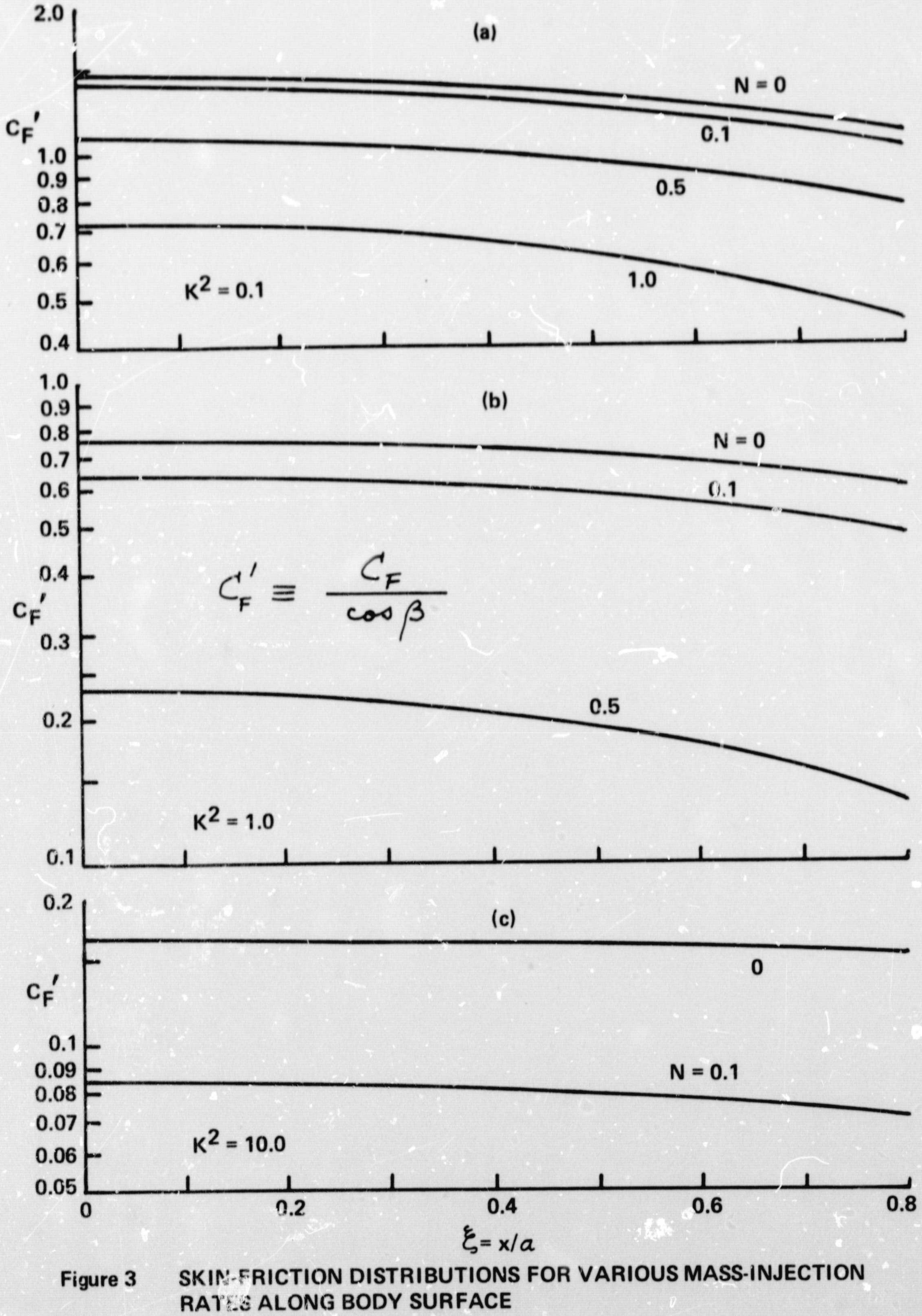

Figure 3 SKIN-FRICTION DISTRIBUTIONS FOR VARIOUS MASS-INJECTION RATES ALONG BODY SURFACE

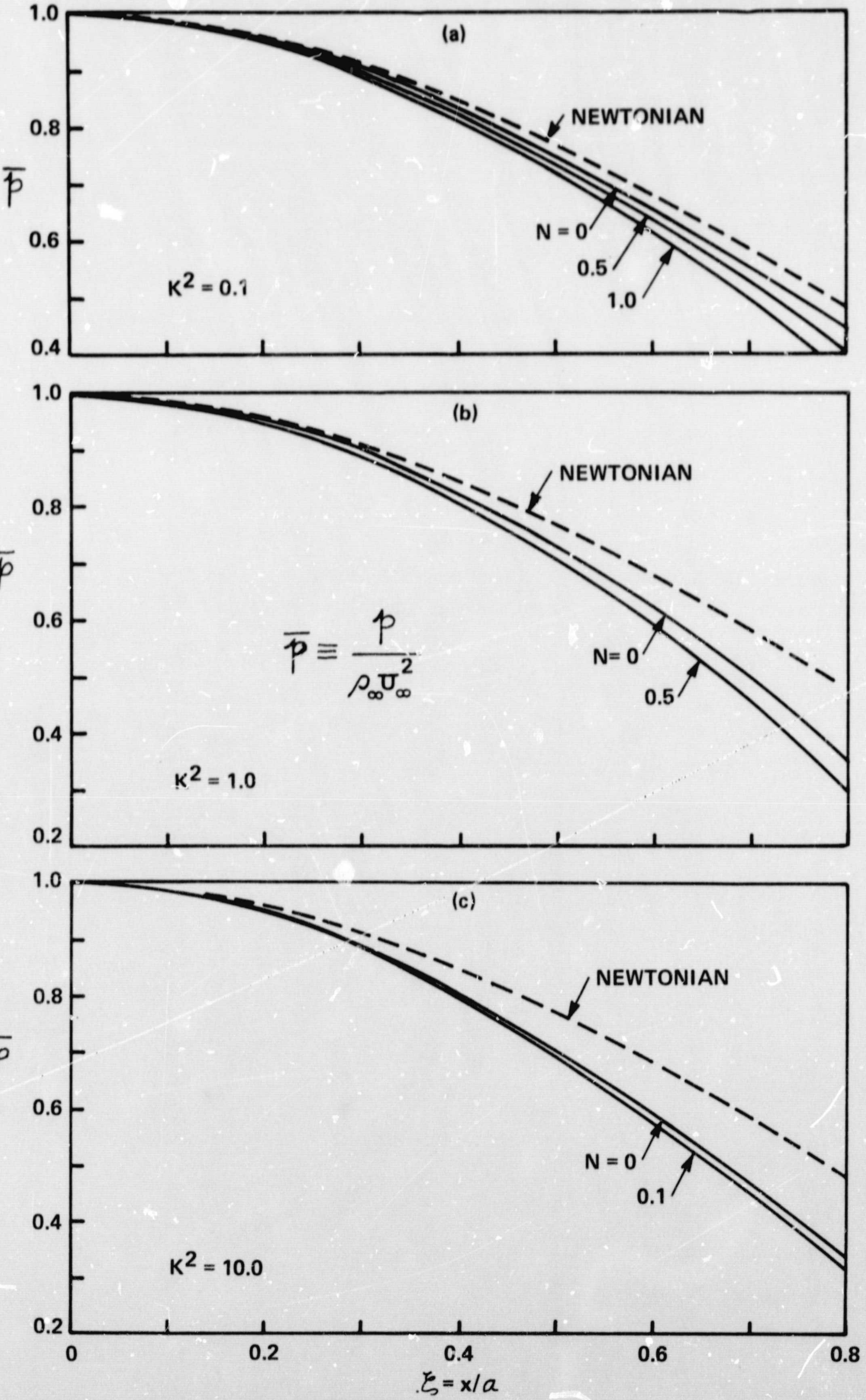

Figure 4 SURFACE-PRESSURE DISTRIBUTIONS FOR VARIOUS MASS-INJECTION RATES ALONG BODY SURFACE

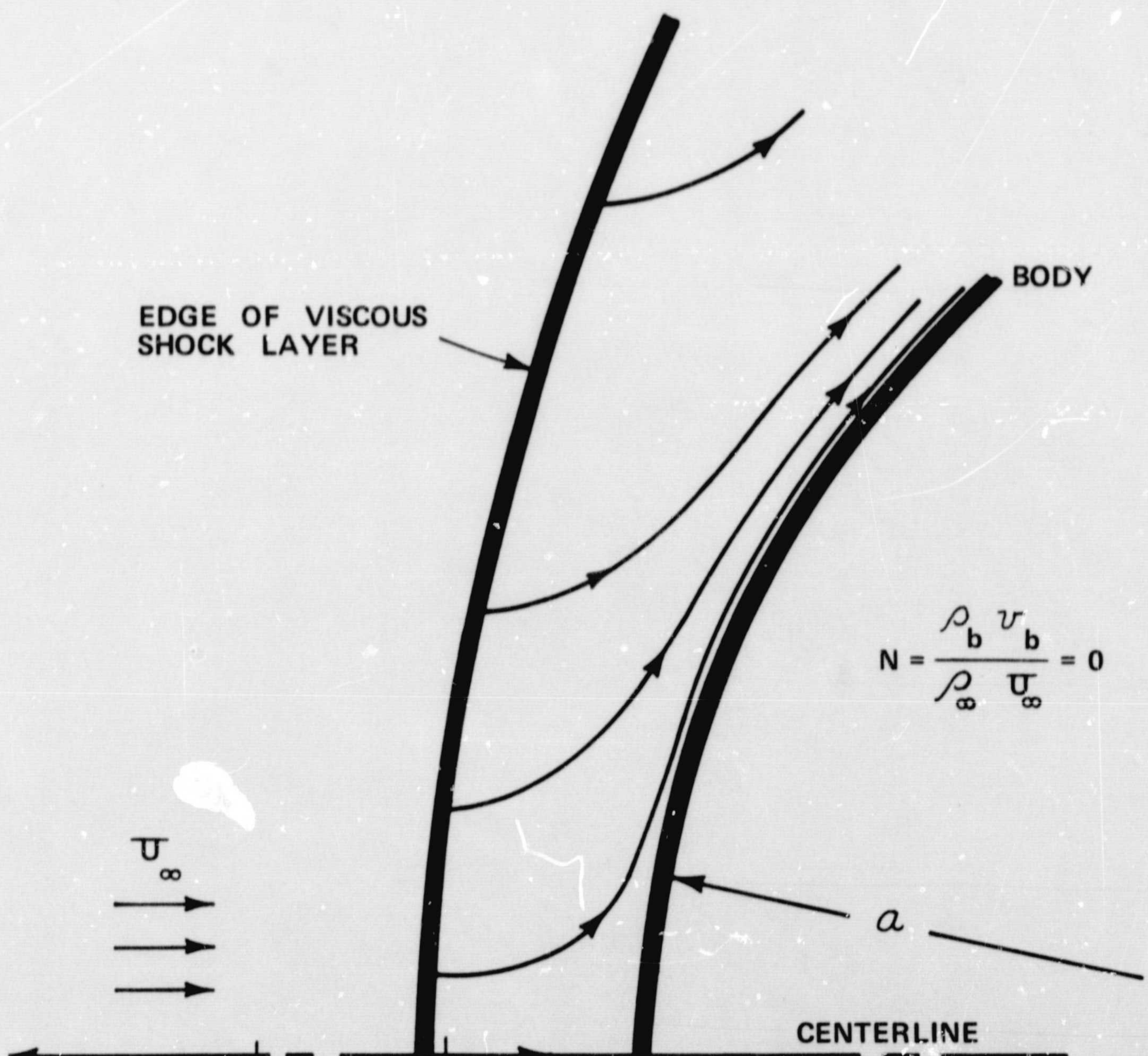

Figure 5 STREAMLINE PATTERNS WITH ZERO MASS INJECTION
($N = 0$, $K^2 = 1.0$, $\mathcal{E} = 1/8$, $t_b = 0.05$, $Pr = 0.75$)

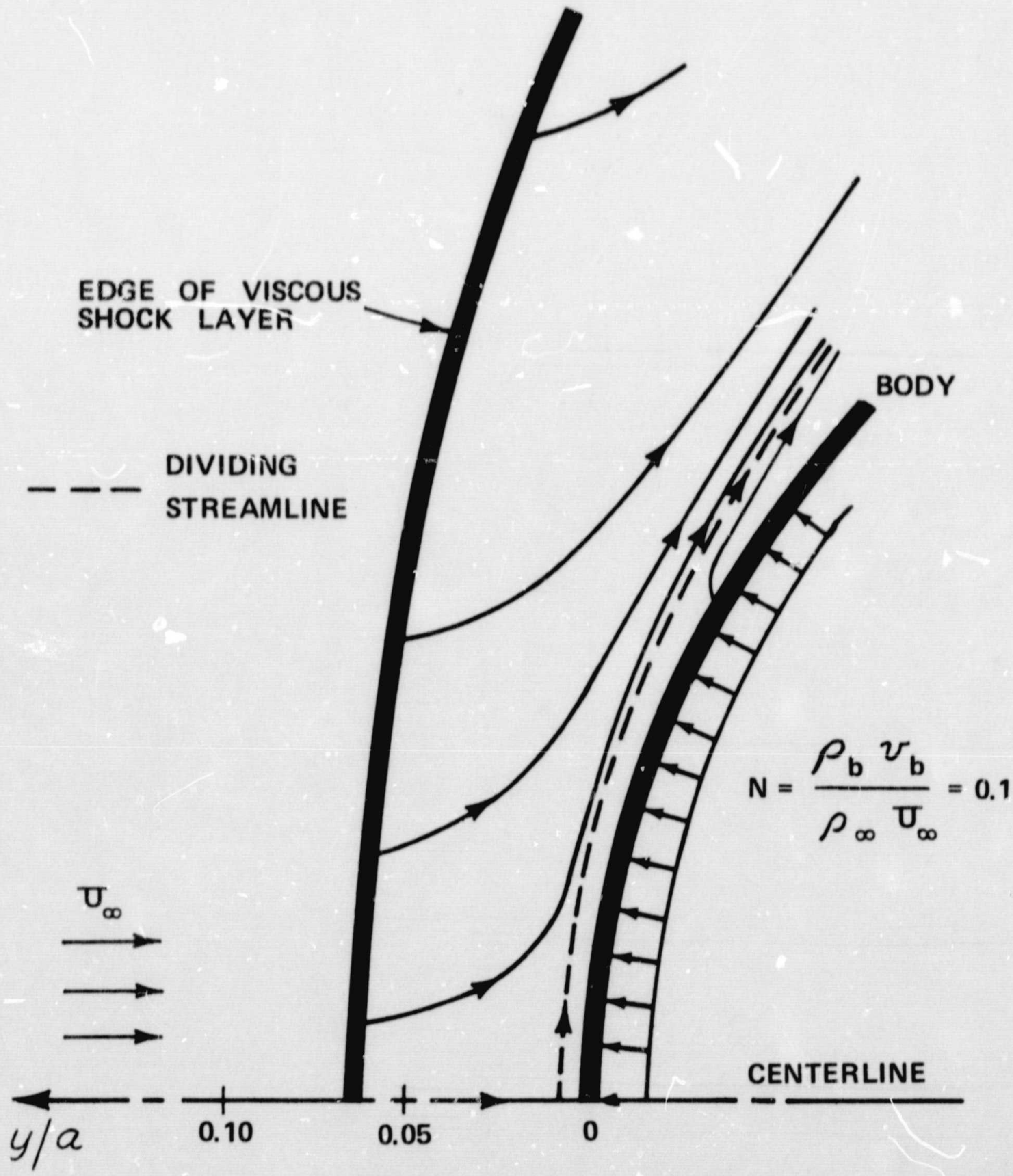

Figure 6 STREAMLINE PATTERNS WITH 10 PERCENT UNIFORM MASS INJECTION ($N = 0.1$, $K^2 = 1.0$, $\varepsilon = 1/8$, $t_b = 0.05$, $Pr = 0.75$)

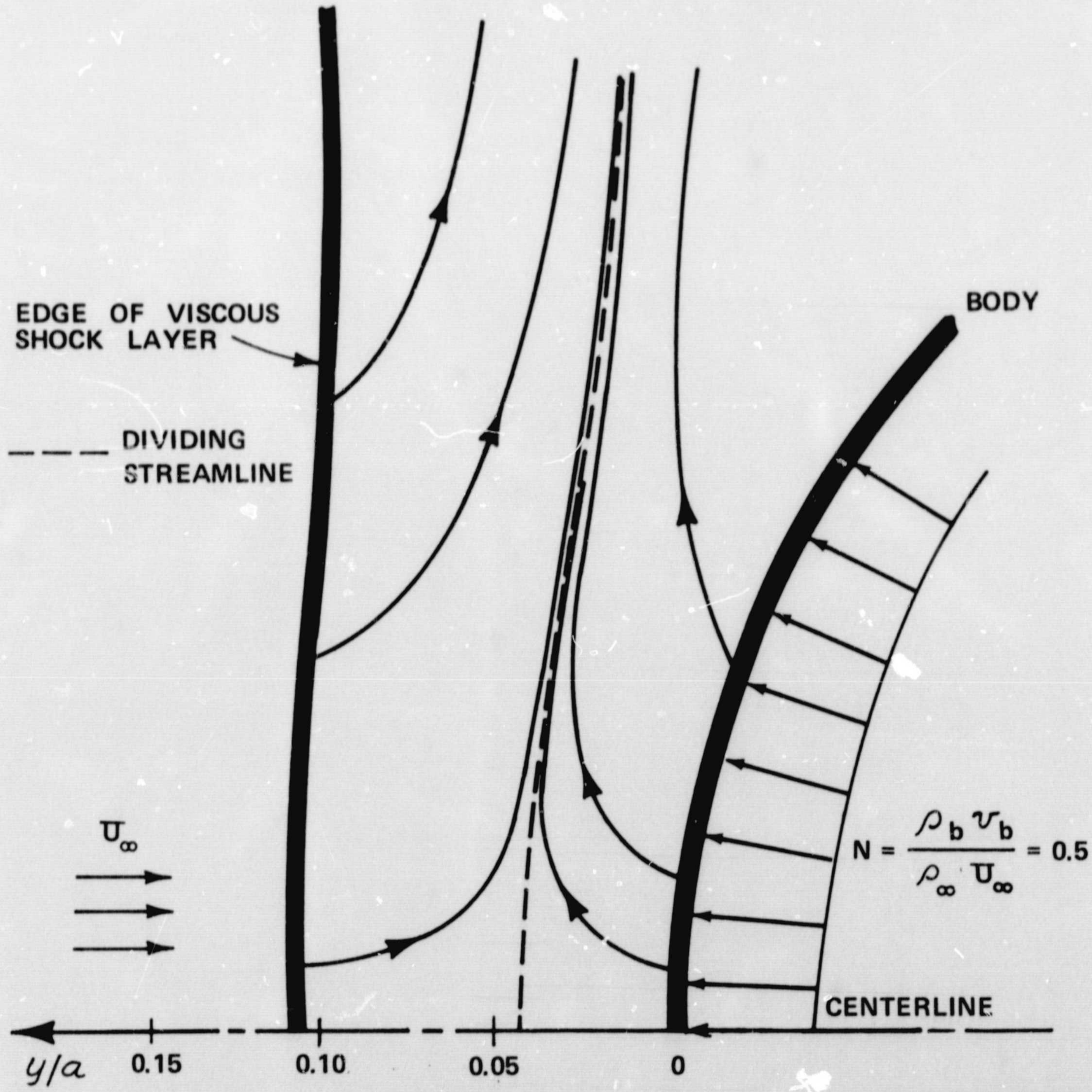

Figure 7 STREAMLINE PATTERNS WITH 50 PERCENT UNIFORM MASS INJECTION
($N = 0.5$, $K^2 = 1.0$, $\varepsilon = 1/8$, $t_b = 0.05$, $Pr = 0.75$)

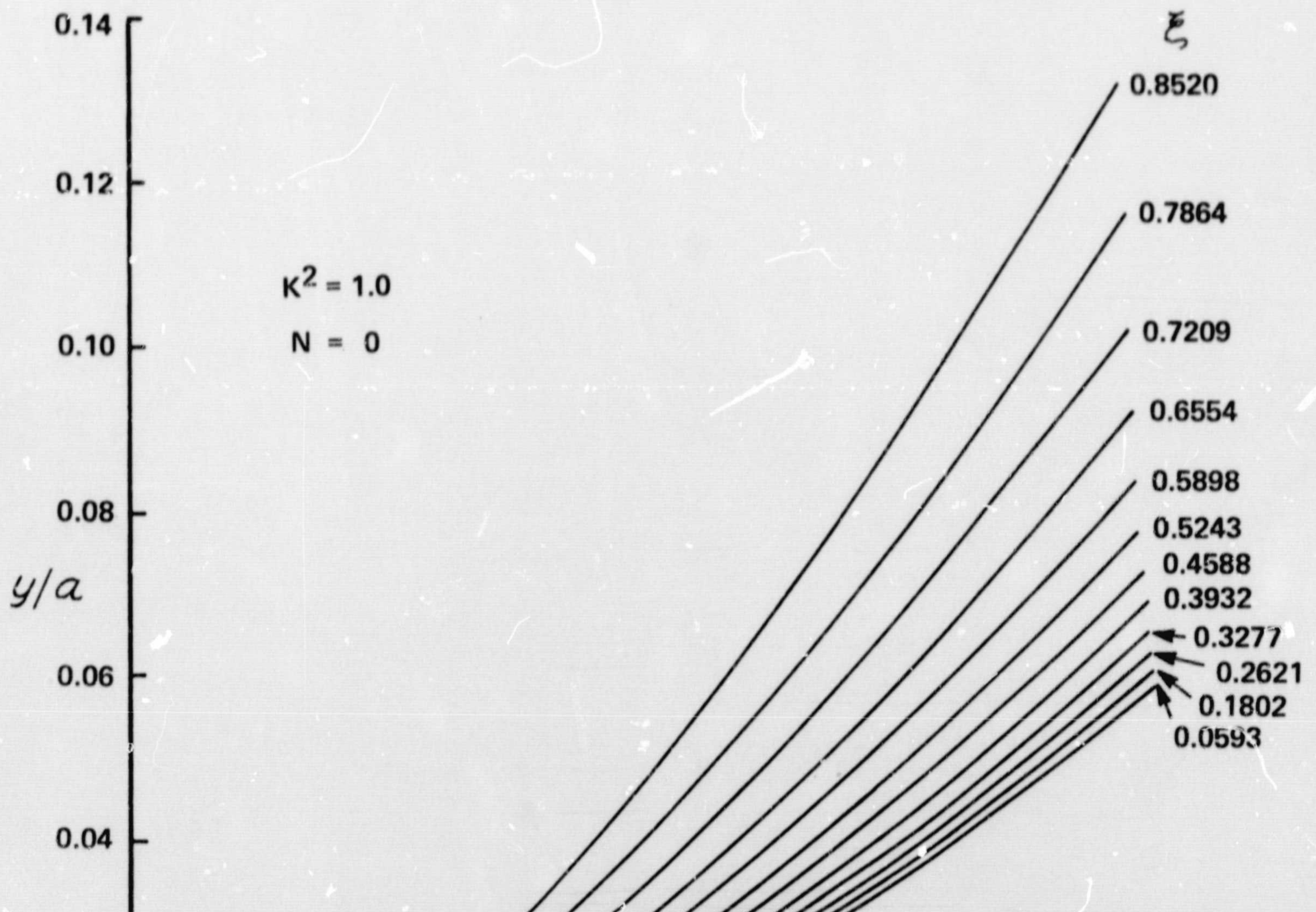

Figure 8 DISTRIBUTIONS OF THE STREAMWISE VELOCITY PROFILES ALONG THE BODY SURFACE WITH ZERO MASS INJECTION

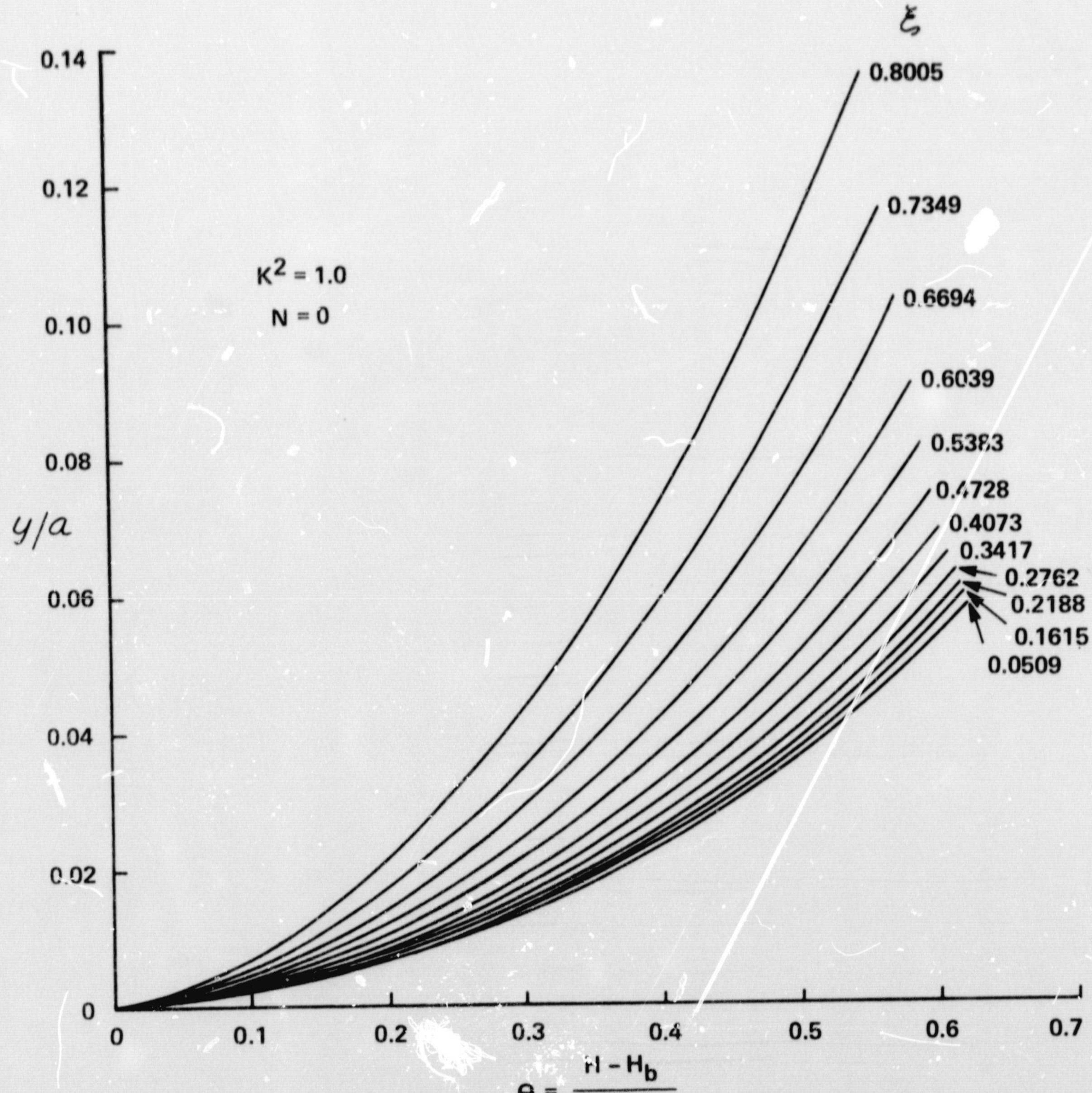

Figure 9 DISTRIBUTIONS OF THE TOTAL-ENTHALPY PROFILES ALONG THE BODY SURFACE WITH ZERO MASS INJECTION

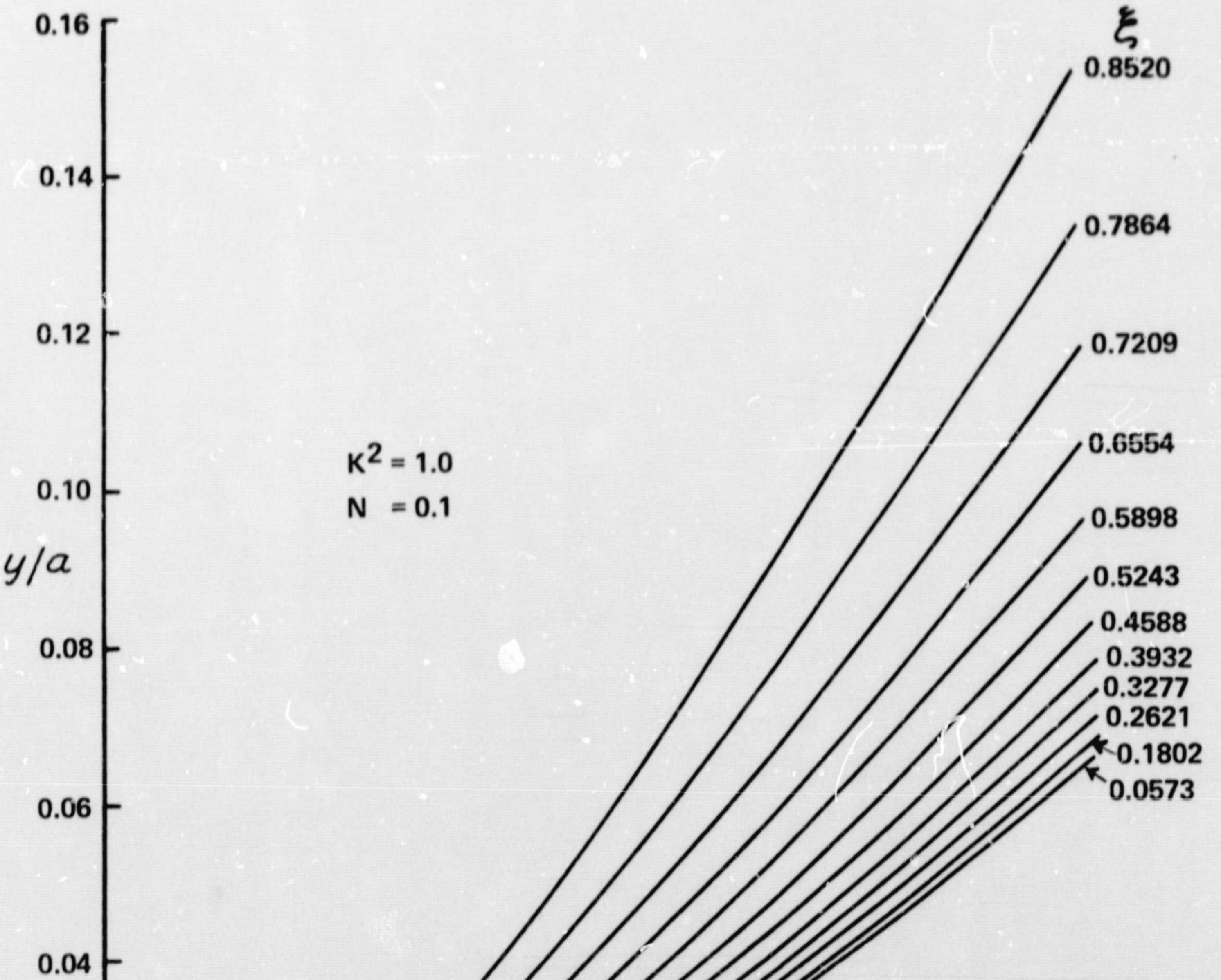

Figure 10 DISTRIBUTIONS OF THE STREAMWISE VELOCITY PROFILES ALONG THE BODY SURFACE WITH 10 PERCENT MASS INJECTION

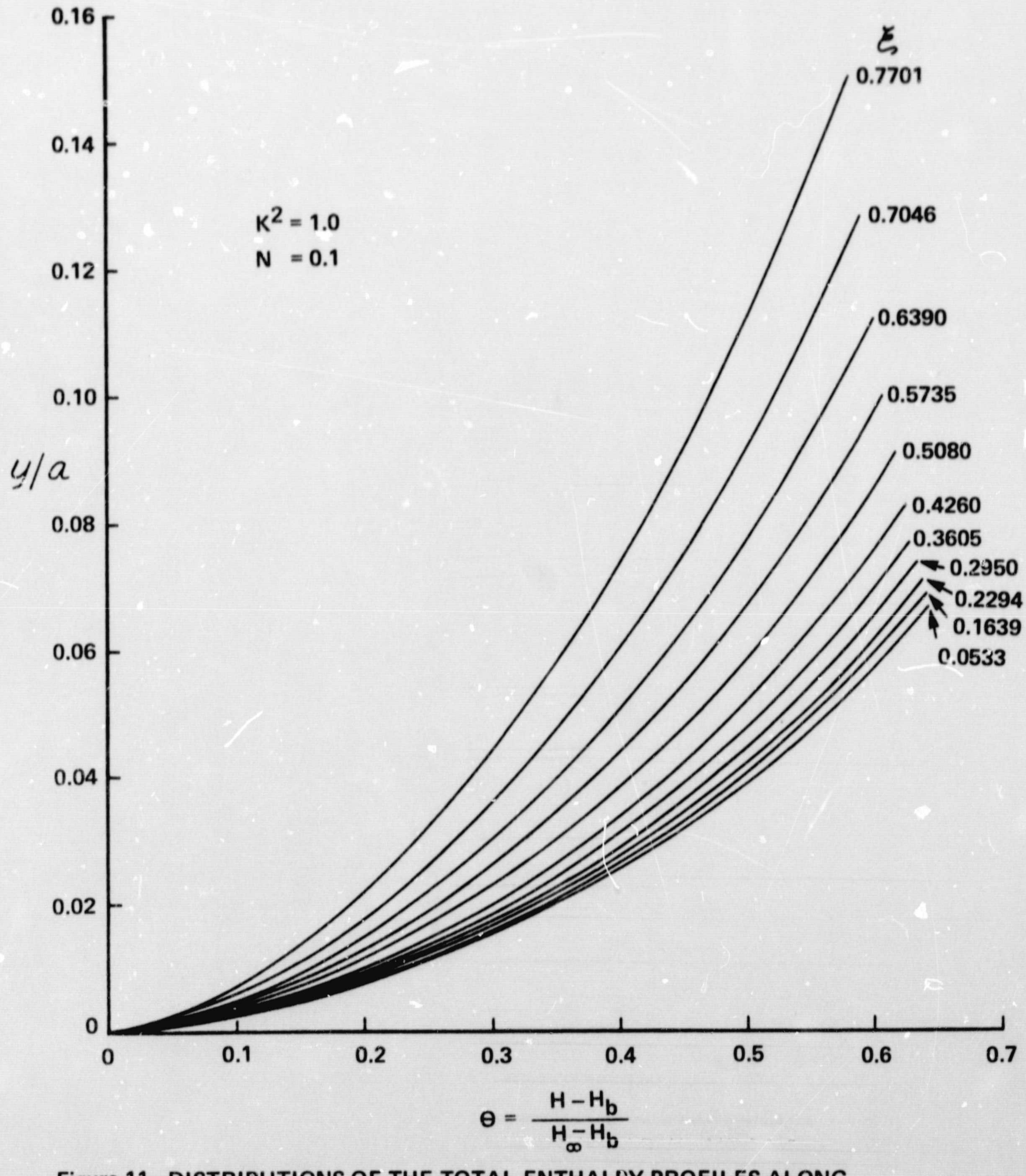

Figure 11 DISTRIBUTIONS OF THE TOTAL-ENTHALPY PROFILES ALONG BODY SURFACE WITH 10 PERCENT MASS INJECTION

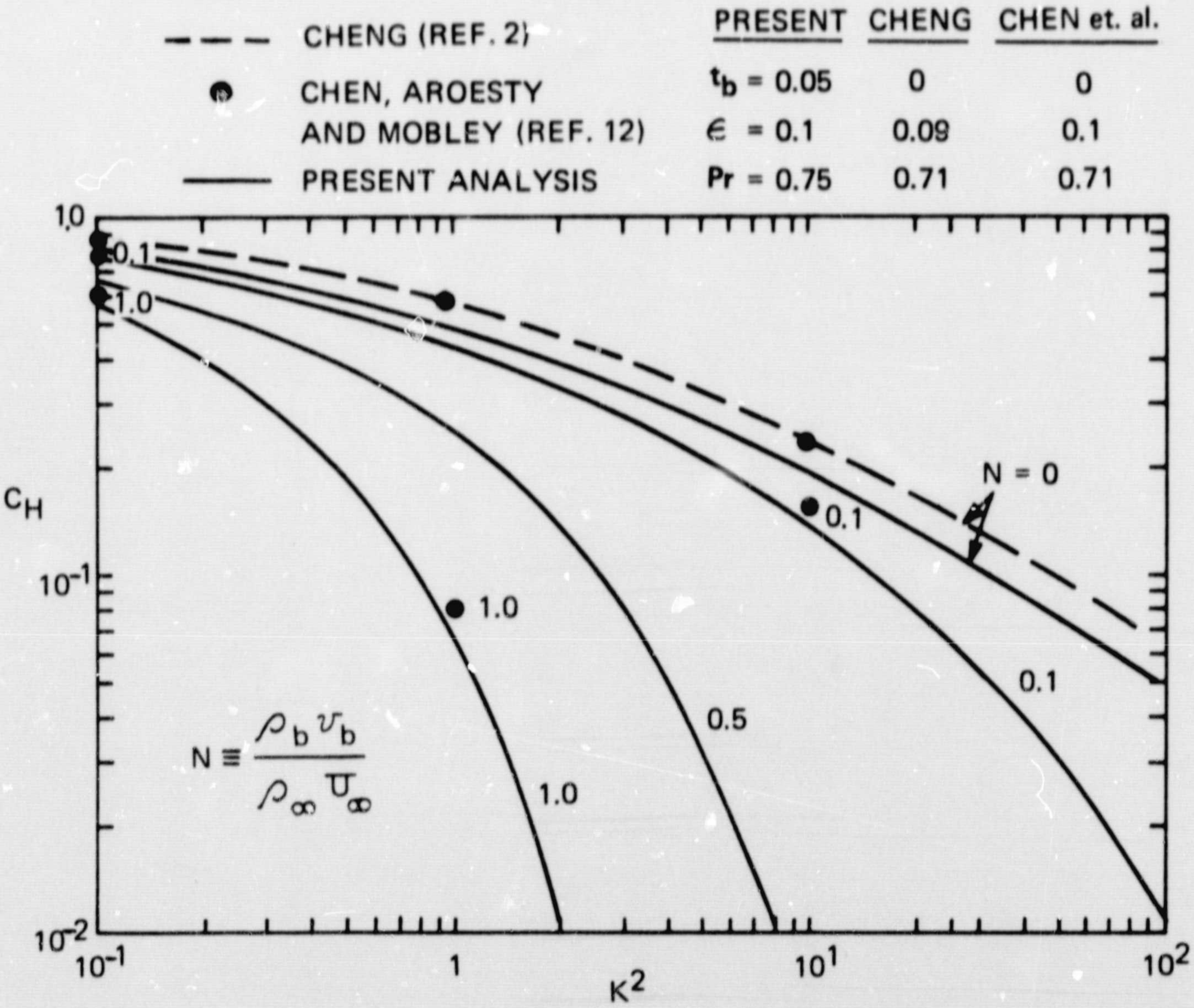

Figure 12 HEAT-TRANSFER RATES AT AN AXISYMMETRIC STAGNATION POINT AT LOW REYNOLDS NUMBER FOR VARIOUS MASS-INJECTION RATES, AND THEIR COMPARISONS WITH EXACT (NUMERICAL) SOLUTIONS.

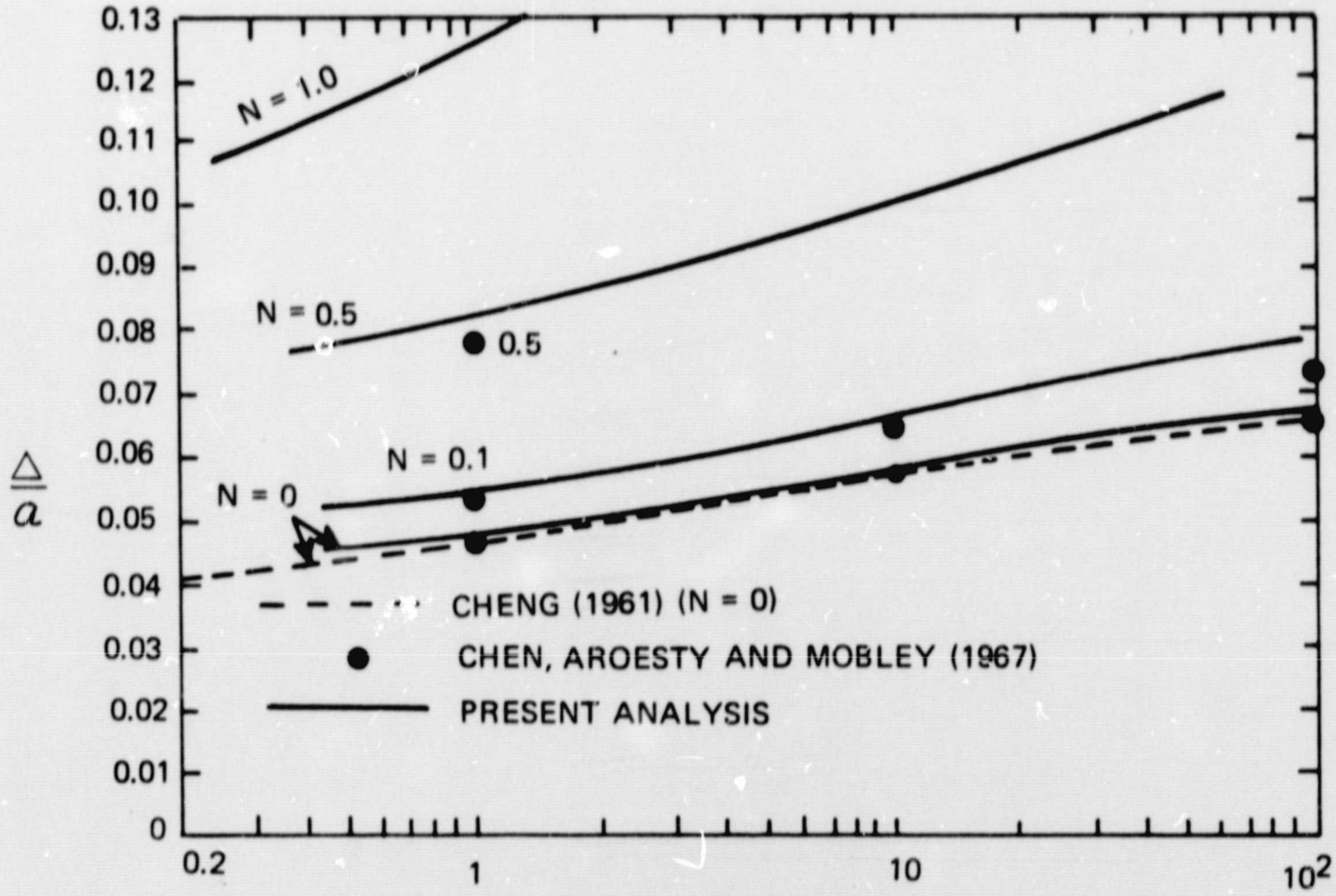

Figure 13 THE SHOCK STAND-OFF DISTANCE FOR THE AXISYMMETRIC STAGNATION POINT FOR VARIOUS MASS-INJECTION RATES, AND ITS COMPARISON WITH EXACT (NUMERICAL) SOLUTIONS.

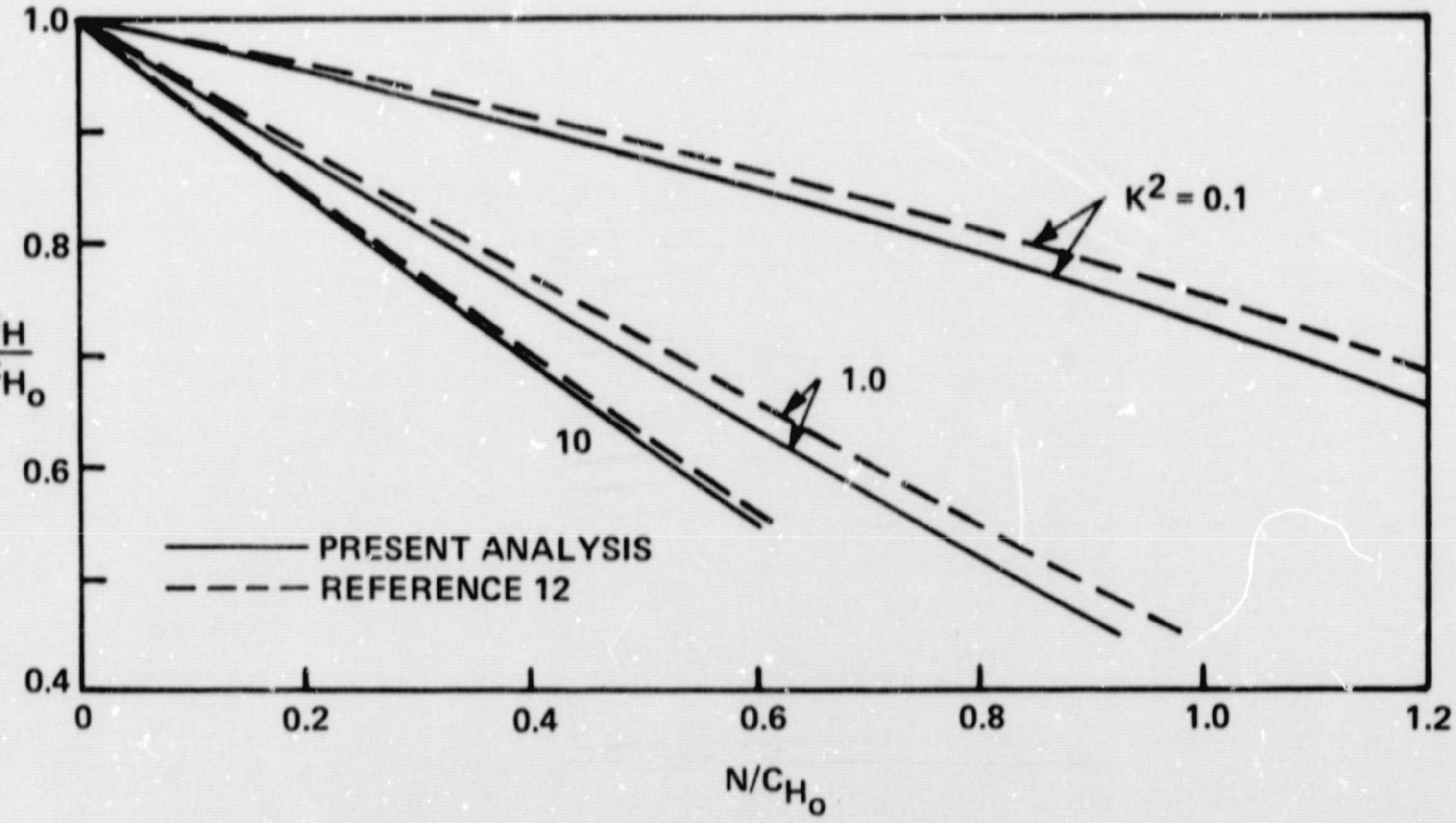

Figure 14 COMPARISON OF CALCULATED HEAT-TRANSFER RATES WITH EXACT (NUMERICAL) SOLUTIONS IN THE STAGNATION REGION. C_{H_o}: HEAT-TRANSFER COEFFICIENT WITH ZERO MASS INJECTION